Ergod. Th. & Dynam. Sys. (1985), **5**, 341–372
Printed in Great Britain

Super persistent chaotic transients

CELSO GREBOGI[1], EDWARD OTT[1,2] AND JAMES A. YORKE[3]

[1] *Laboratory for Plasma and Fusion Energy Studies and Department of Physics and Astronomy,* [2] *Department of Electrical Engineering*; [3] *Institute for Physical Science and Technology and Department of Mathematics*; *University of Maryland, College Park, Maryland* 20742, *USA*

(*Received* 1 *December* 1984)

Abstract. The unstable-unstable pair bifurcation is a bifurcation in which two unstable fixed points or periodic orbits of the same period coalesce and disappear as a system paremeter is raised. For parameter values just above that at which unstable orbits are destroyed there can be chaotic transients. Then, as the bifurcation is approached from above, the average length of a chaotic transient diverges, and, below the bifurcation point, the chaotic transient may be regarded as having been converted into a chaotic attractor. It is argued that unstable-unstable pair bifurcations should be expected to occur commonly in dynamical systems. This bifurcation is an example of the crisis route to chaos. The most striking fact about unstable-unstable pair bifurcation crises is that long chaotic transients persist even for parameter values relatively far from the bifurcation point. These long-lived chaotic transients may prevent the time asymptotic state from being reached during experiments. An expression giving a lower bound for the average lifetime of a chaotic transient is derived and shown to agree well with numerical experiments. In particular, this bound on the average lifetime, $\langle\tau\rangle$, satisfies

$$\langle\tau\rangle \geq k_1 \exp\left[k_2(\alpha-\alpha_*)^{-1/2}\right]$$

for α near α_*, where k_1 and k_2 are constants and α_* is the value of the parameter α at which the crisis occurs. Thus, as α approaches α_* from above, $\langle\tau\rangle$ increases more rapidly than any power of $(\alpha-\alpha_*)^{-1}$. Finally, we discuss the effect of adding bounded noise (small random perturbations) on these phenomena and argue that the chaotic transients should be lengthened by noise.

1. *Introduction*

Recently, the subject of chaotic motions of dynamical systems has generated a great deal of interest. This interest has been stimulated both by recent fundamental advances in theory and by clear and striking applications to the interpretation of experiments in many fields of science [**8**]. Much current interest in the field has been concerned with identifying typical bifurcations associated with chaotic attractors [**1**]–[**5**], [**9**] (e.g. period doubling cascades and intermittency.) In this paper we discuss a new type of dynamical bifurcation phenomenon leading to chaos, and we describe the basin boundaries and chaotic transients associated with it. We call this bifurcation the unstable-unstable pair bifurcation [**4**].

(A) *The unstable-unstable pair bifurcation and its associated chaotic dynamics—summary of phenomena.* In an unstable-unstable pair bifurcation two unstable orbits are destroyed. The process occurs as follows. We imagine that as a parameter of the system is raised, approaching its bifurcation value, the two unstable orbits move toward each other, coalesce at the bifurcation value and disappear above it.

For parameter values just after the destruction of the unstable pair of orbits there is a chaotic transient. (If there is a chaotic transient, then the motion initially appears to be chaotic, but only lasts a finite time, after which it suddenly approaches some distant attractor. The duration τ of chaotic transients depends quite sensitively on the initial conditions and, with even very small uncertainty in the initial conditions, this duration may be thought of as being randomly distributed with an exponential distribution $\sim\exp(-\tau/\langle\tau\rangle)$, where $\langle\tau\rangle$ denotes the average value of τ.) However, we note that these chaotic transients exist only for initial conditions in a restricted region of the phase space. For initial conditions outside this region, the generated orbit appears to immediately move away from this region, generally approaching a distant attractor. For convenience, in the examples in this paper, the distant attractor is the point at infinity. We note, however, that changes in the dynamics of our examples can be introduced which convert the attractor at infinity to an ordinary attractor (e.g. a periodic orbit). The most striking aspect of this type of event is *the extraordinary persistence of the chaotic transients* that are observed. In particular, they are very long even when system parameters deviate substantially from their values at the unstable-unstable pair bifurcation.

Now imagine that a parameter of the system is decreased. As it approaches its value at the unstable-unstable pair bifurcation the average length of a chaotic transient diverges. Below the bifurcation there is a chaotic attractor, which can be regarded as having arisen by conversion from the chaotic transient. In addition, the distant attractor which existed after the bifurcation (for our examples, the point at infinity) is still present. Each of these attractors has its own basin of attraction (a *basin of attraction* is the closure of the set of initial conditions which yield orbits that approach the attractor asymptotically with time; a point is in the *basin boundary* if it is in the closure of two or more basins). For the examples we present here, the basin boundaries are curves or surfaces which appear to be nowhere differentiable and have non-integer (fractal) dimension.

At the unstable-unstable pair bifurcation point the two unstable orbits coincide. As the system parameter is decreased below its bifurcation value, the two unstable orbits separate in phase space. For our examples, we find that one of the unstable orbits lies in the chaotic attractor and that the chaotic attractor is the closure of the unstable manifold emanating from that orbit. In addition, the other unstable orbit lies on the basin boundary.

Now imagine that the chaotic attractor exists and vary the system parameter in the other direction (i.e. so that the bifurcation is again approached). Viewing the situation in phase space, one would observe that the chaotic attractor and basin boundary approach each other and first touch at the point of bifurcation where the two unstable orbits coalesce. Past this point, the unstable orbit pair no longer exists,

and the chaotic attractor is destroyed and replaced by the chaotic transient. However, in a sense, the chaotic transient is a remnant of the chaotic attractor. In particular, the initial conditions which yield chaotic transients lie in the region of the former basin of attraction of the chaotic attractor, and the orbit in the chaotic transient phase appears to be similar (although only for the finite time of the transient) to that of the chaotic attractor. In addition, trajectories with initial conditions in the region of the old basin of attraction of the other attractor are unaffected and do not experience chaotic transients.

(B) *Remarks.* (1) In [**3**] and [**5**] it was conjectured that in some sense 'almost all' sudden deaths of chaotic attractors that occur as a system parameter is varied result from a collision of the attractor with an unstable periodic or quasiperiodic orbit on the basin boundary, and this type of occurrence was called a *boundary crisis.* (Whether or not the conjecture is true, this kind of event is extremely common.) The destruction of the chaotic attractor in the case of an unstable-unstable pair bifurcation is a boundary crisis, since the attractor hits the basin boundary at the coalescence of the two unstable orbits, one of which is on the basin boundary. Note that this is a fundamentally different kind of boundary crisis from the boundary crises of the Lorenz attractor and Henon map [**5**]. In numerical studies of these latter cases, the crisis is seen to occur when there is a homoclinic tangency of a saddle-periodic orbit on the basin boundary.

(2) There appear to be basically two kinds of routes to chaos (i.e. mechanisms by which chaotic attractors can come about). In the first kind, called scenarios by Eckmann, [**1**], a non-chaotic attractor *evolves* into a chaotic attractor. Examples of scenarios include period doubling cascades [**2**], and intermittency [**9**]. In the second kind, called crises by us [**3**], [**5**], a chaotic attractor appears by conversion of a chaotic transient. The appearance of a chaotic attractor in an unstable-unstable pair bifurcation is an example of the crisis route to chaos.

(3) Perhaps the most interesting aspect of the unstable-unstable pair bifurcation crisis is the extreme persistence of long chaotic transients with variation of system parameters. This is in contrast with the chaotic transients associated with other types of crises [**3**], [**5**]. To get an idea of the numbers involved, we note that, for the mapping considered in § 3, the average duration of a chaotic transient is still $>10^7$ when the system parameter deviates from its value at the crisis by 12%.

(4) It follows from remark 3 that an experimenter might need to carry out an experiment for a very long time to be able to distinguish a real chaotic attractor from a chaotic transient; chaos can persist for a long time, and telling the difference may in some circumstances be impractical or irrelevant.

(C) *Outline of the rest of this paper.* In § 2 we demonstrate the unstable-unstable pair bifurcation crisis using a two-dimensional non-invertible map. We observe, for this map, that the basin boundary appears to be a fractal curve. For a value of the parameter below the crisis value there are two attractors, one chaotic and one non-chaotic (for this case the non-chaotic attractor is the point at infinity). As the parameter is raised, a crisis occurs in which a repeller fixed point on the basin boundary

and a saddle fixed point on the chaotic attractor collide. We derive a formula for the average lifetime of this chaotic transient and compare it with numerical results.

In § 3, we study a three-dimensional map displaying similar phenomena. For this map the chaotic attractor appears to be a nowhere differentiable torus. The basin boundary is another fractal toroidal surface surrounding the attractor. As a parameter of the system is raised a crisis occurs in which unstable fixed points on the two tori coalesce. The unstable point on the attractor has a one-dimensional unstable manifold and two-dimensional stable manifold, while the unstable point on its basin boundary has a one-dimensional stable manifold and a two-dimensional unstable manifold. Evidently, the closure of the unstable manifold of the first point is the fractal torus chaotic attractor, while the closure of the stable manifold of the second point is a fractal torus repeller which is the basin boundary for the attractor. Each one of these fractal toroidal surfaces has one smooth direction, that of the unstable manifold for the attractor and that of the stable manifold for the basin boundary. Above the crisis value of the parameter, almost all initial conditions eventually asymptote to infinity – although there are chaotic transients. The average length of the chaotic transient is also very long, as in the two-dimensional case (see § 2).

In § 4 we provide a rigorous mathematical argument showing that the unstable-unstable pair bifurcation and the associated long-lived chaotic transients are not particular to the examples presented here, but represent a common behaviour in non-linear dynamics.

In § 5 we discuss the effect of bounded noise on the long-lived chaotic transients. The significant result is that the super long chaotic transients persist in the presence of bounded noise. In fact, we argue that, in a suitable sense, the effect of noise is to increase the duration of the chaotic transient.

2. *Long-lived chaotic transients in a two-dimensional non-invertible map*

To illustrate the unstable-unstable pair bifurcation to chaos and the associated long chaotic transients, we start with the non-invertible two-dimensional map given by

$$\theta_{n+1} = 2\theta_n, \qquad \text{mod } 2\pi, \tag{1a}$$

$$z_{n+1} = \alpha z_n + z_n^2 + \beta \cos \theta_n. \tag{1b}$$

There are two fixed points, namely, $(0, z_b)$ and $(0, z_c)$ on the basin boundary and chaotic attractor, respectively, as shown in figure 1, $z_b = (1-\alpha-r)/2$ and $z_c = (1-\alpha+r)/2$, where $r = [(1-\alpha)^2 - 4\beta]^{\frac{1}{2}}$. Equation (1a) is the two-shift map defined in $[0, 2\pi)$. In (1b), β is the strength of the coupling between θ and z evolutions, and α is the parameter which we wish to vary. Figure 1 shows a picture obtained by iterating equations (1) for $\alpha = 0.5$ and $\beta = 0.04$. For these parameters there are apparently two attractors, one which is chaotic and the other at $z = +\infty$. The basins of attraction are determined by choosing a grid of 260 000 points in the frame of the picture and iterating each of them up to 150 times. If a given orbit goes to large positive z values, we plot a black dot for the initial condition of that orbit. If an orbit remains bounded ($z < 0.6$) we leave the grid point blank. We shall argue that

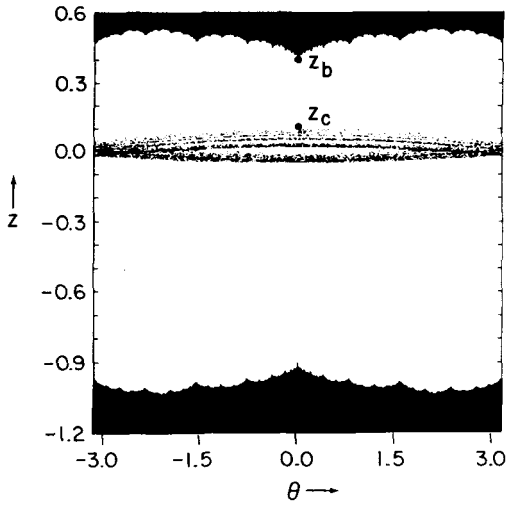

FIGURE 1. A chaotic trajectory and the attractor's basin of attraction for $\alpha = 0.50$ and $\beta = 0.04$. Trajectories initialized in the dark region asymptote to $z = +\infty$, while trajectories initialized in the blank region are attracted to the chaotic attractor. In order to more clearly display the collision of the chaotic attractor and its basin boundary, which occurs at $\theta = 0$, we have plotted θ on $(-\pi, \pi)$ rather than on $(0, 2\pi)$.

the boundary between the black and the blank regions is a fractal curve. The chaotic attractor is added to this picture by choosing a single initial condition in the blank region. For that initial condition we preiterate the map 5000 times (to eliminate the initial transient effect), and then we plot the next 10 000 iterates, as shown in figure 1.

To see that $z = +\infty$ is an attractor, we note from (1b) that for large $|z|$, $z_{n+1} > z_n^2$. Thus, points with sufficiently large $|z|$ have trajectories that asymptote to $z = +\infty$. It is useful to regard $z = +\infty$ as representing a general attractor, since other terms could be added to the map, equation (1b), to prevent the orbit from going to $z = +\infty$ but which would leave unchanged the phenomena associated with the chaotic attractor and its basin boundary.

To understand why there is a chaotic attractor in figure 1, we note that $\theta = 0$, $z_c = 0.1$ is a fixed point, and the band $|z| \leq 0.1 = z_c$ is mapped onto itself. Since the dynamics in θ is chaotic, there is a chaotic attractor located in the region $-0.1 \lesssim z \lesssim 0.1$. The Lyapunov numbers for this attractor can be estimated by utilizing the following approximation to the dynamics. We linearize equation (1b) about $z = 0$ and by setting $z = \beta\delta$. We obtain

$$\theta_{n+1} = 2\theta_n, \qquad \mod 2\pi, \tag{2a}$$

$$\delta_{n+1} = \lambda\delta_n + \cos\theta_n, \tag{2b}$$

with $\lambda = 0.5$ yielding the Lyapunov numbers 2 and λ. The map (2) has been investigated in [4] and [7].

The same crude argument can be used to make plausible the presence of the upper fractal basin boundary for equations (1) located in the region $\frac{1}{2} \lesssim z \lesssim$

https://doi.org/10.1017/S014338570000300X Published online by Cambridge University Press

$(1-\alpha+r)/2 \simeq 0.64$, where $r=[(1-\alpha)^2+4\beta]^{\frac{1}{2}}$. The upper basin boundary must be located in this region since every initial point chosen above that band has z_n strictly monotonically increasing with $z_n \to \infty$, and $z_{n+1} \geq \lambda z_n + z_n^2 - \beta$. Each vertical line segment in this band is mapped to a longer vertical line segment that stretches across the band. Since in this band the map is expansive in the z direction [i.e. $(\partial/\partial z_n) \times (\alpha z_n + z_n^2 + \beta \cos \theta_n) > 1$], there will be a unique point $z(\theta)$ on each of these segments that remain in the band for all time. This surface $[(\theta, z(\theta))]$ (topologically a circle) is invariant by definition, and it separates the basins of ∞ and the bounded attractor below it. We now give a heuristic argument that $z(\theta)$ is a nowhere differentiable curve. Linearization of the z map about $z=0.5$ by setting $z=\beta\delta+0.5$ yields the map (2) with $\lambda=1.5$. In this case $(1<\lambda<2)$, we have shown [4] that the map (2) has a nowhere differentiable invariant curve

$$\delta = \sigma(\theta) = -\sum_{k=1}^{\infty} \lambda^{-(k+1)} \cos(2^k\theta). \tag{3}$$

Since $\lambda > 1$, the sum converges absolutely and uniformly. Initial points (θ, δ) above the curve (3) tend to $\delta = +\infty$ while points below tend to $-\infty$. It is thus plausible that the upper basin boundary of equations (1) is also a nowhere differentiable curve. The lower basin boundary in the vicinity of $z=-1.0$ would also be a fractal curve, being essentially a pre-image of the upper basin boundary. Each point in the lower black region is mapped in one iterate into the upper black region after which it remains positive. Figure 2 shows a magnification of the state space containing the upper basin boundary. Figure 3 shows a magnification of the boxed region indicated in figure 2 illustrating the fractal structure of the upper basin boundary.

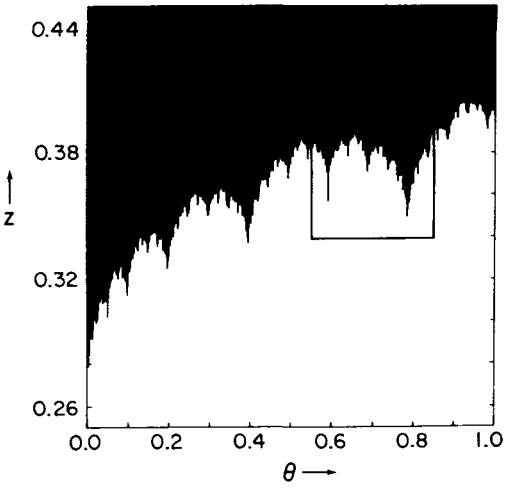

FIGURE 2. Magnification of a small portion of the state space showing the fractal basin boundary.

Now we consider what happens as we increase the parameter α from $\alpha=0.5$. As we increase α the chaotic attractor reaches a crisis [4] at $\alpha=0.6$. As seen in figure 1, the smallest z value on the upper basin boundary occurs at $\theta=0$ and $z=z_b$, and

https://doi.org/10.1017/S014338570000300X Published online by Cambridge University Press

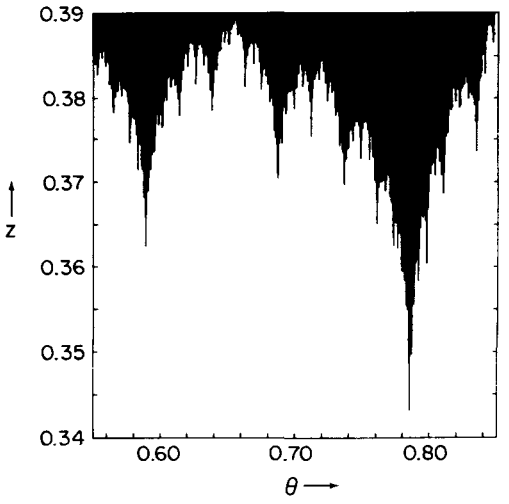

FIGURE 3. Further magnification of the boxed region in figure 2 illustrating the fractal structure of the basin boundary.

the largest z value on the chaotic attractor occurs at $\theta = 0$ and $z = z_c$. The reason for this is that the cos θ term in equation (1b) is maximum for $\theta = 0$ which is a fixed point of equation (1a). Linearization of the map (1) about these two fixed points shows that they are unstable. As shown schematically in figure 4, $(0, z_b)$ is a repeller having two unstable directions, while $(0, z_c)$ is a saddle having one direction attracting and another repelling. As α increases the two points $(0, z_b)$ and $(0, z_c)$ move close together until at some critical value $\alpha = \alpha_*$, they first touch. From (1b) we have

$$\alpha_* = 1 - 2\beta^{\frac{1}{2}}. \tag{4}$$

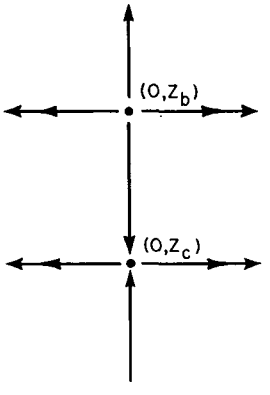

FIGURE 4. Illustration of the unstable pair. $(0, z_b)$ is unstable in two directions. $(0, z_c)$ is stable in one direction and unstable in the other direction. The chaotic attractor apparently is the closure of the unstable manifold emanating from $(0, z_c)$.

https://doi.org/10.1017/S014338570000300X Published online by Cambridge University Press

Hence, $\alpha_* = 0.6$ for $\beta = 0.04$. For $\alpha > \alpha_*$ the chaotic attractor and its basin of attraction, as well as the two fixed points, no longer exist. Conversely, as α decreases through $\alpha = \alpha_*$, the unstable fixed point pair and the strange attractor and its basin are born via the unstable-unstable pair bifurcation.

We now claim that for almost every initial θ_0 (independent of the choice of the initial z_0), we have $z_n \to \infty$ for $\alpha > \alpha_*$. For $\theta = 0$ and any initial z_0, we have $z_{n+1} = \alpha z_n + z_n^2 + \beta > z_n$ and z must go to ∞. It is not hard to see that there is a value n_* such that $z_{n_*} > 2$ for every initial value z_0 with $\theta = 0$. Now let (θ_0, z_0) be any initial condition for which the values θ_n are dense in $[0, 2\pi]$. It follows that there is some ε such that when $|\theta_n| < \varepsilon$, after n_* iterates we have $z_{n+n_*} > 2$, and then $z_n \to \infty$ monotonically. In particular, the set of points going to $z = +\infty$ is open and dense.

Although our example, equations (1), exhibits the phenomenon of unstable-unstable pair bifurcation to chaos for the case in which the pair is a pair of fixed points, we emphasize that the same considerations apply when the pair is a pair of periodic orbits. For instance, for $\beta = -0.08$ we apparently obtain a crisis with annihilation of orbits of period 2 at $\alpha = \alpha_* = 0.6$, with $\theta = \pm 2\pi/3$ as shown in figure 5. Unlike the previous case, we have no rigorous argument that the basin boundary

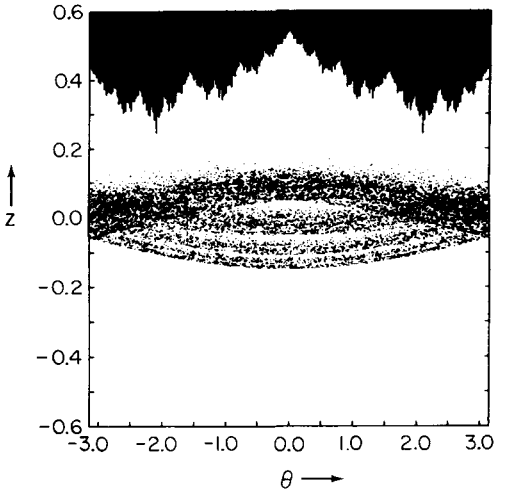

FIGURE 5. Picture of the chaotic attractor and its basin of attraction (blank region) for $\alpha = 0.6$ and $\beta = -0.08$ showing a period 2 crisis. Observe that the smallest z value in the upper basin boundary occurs at $\theta = \pm 2\pi/3$. See caption of figure 1 for the definition of the abscissa θ.

first touches the attractor at these two θ values. The period two orbit occurs at $\theta = 2\pi/3, 4\pi/3$, since $2\pi/3 \to 4\pi/3 \to 2\pi/3$. Here we have $\cos\theta = -\frac{1}{2}$. Then, the two coordinates of the period two repeller orbit are $(-2\pi/3, z_b^{(2)})$ and $(2\pi/3, z_b^{(2)})$ while the period two saddle orbit is at $(-2\pi/3, z_c^{(2)})$ and $(2\pi/3, z_c^{(2)})$. Both $z_c^{(2)}$ and $z_b^{(2)}$ satisfy $z = \alpha z + z^2 - \beta/2$. At the crisis there would be a single period two orbit. We set the discriminant equal to zero and obtain $\alpha_* = 1 + (-2\beta)^{\frac{1}{2}}$. (Then, at the crisis $z_b^{(2)} = z_c^{(2)} = 0.2$.)

https://doi.org/10.1017/S014338570000300X Published online by Cambridge University Press

We consider now what happens when the parameter α just exceeds the crisis value α_*. We observe that the chaotic attractor becomes a chaotic transient. Orbits with initial points in the region which was formerly the basin of attraction for the chaotic attractor will typically approach what looks like the old chaotic attractor. The orbit then bounces around in this remnant in an apparently chaotic fashion as it did for $\alpha < \alpha_*$. However, after some time the orbit lands sufficiently near the region where $(0, z_c)$ and $(0, z_b)$ coalesce, and then rapidly leaves the chaotic attractor remnant, accelerating to large positive z values. Hence, the chaotic attractor which exists for $\alpha < \alpha_*$ is replaced by a chaotic transient for $\alpha > \alpha_*$. Figure 6 shows a chaotic transient for $\beta = 0.04$ and $\alpha = 0.65 > \alpha_* = 0.60$. The black region represents

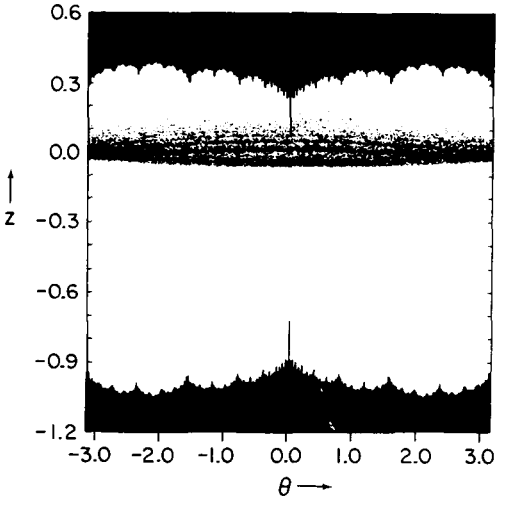

FIGURE 6. Picture of the chaotic transient for $\beta = 0.04$ and $\alpha = 0.65 > \alpha_* = 0.60$. See caption of figure 1 for the definition of the horizontal axis θ. All spikes at $\theta = 2\pi m/2^k$ extend all the way through.

initial points which rapidly acquire large z values in 150 iterates of the map. This picture does not depend strongly on that number since the average length of the chaotic transient appears to be very long ($\sim 2 \times 10^7$ iterates) for these parameters. Also shown in the picture are the first 10^4 iterates of a chaotic transient generated from a single initial condition in the blank region. We note the apparent penetration of the black region into the region of the attractor at $\theta = 0$, the θ value at which the unstable-unstable pair coalesces. In fact, the penetrations of the upper and lower black regions join each other but it was not possible to detect them numerically even though we used more than a quarter of a million initial conditions in the picture. The reason is that the black region spike that pierces the attractor is very narrow, which expains the very long transients. Indeed all the spikes at $\theta = 2\pi m/2^k$, for integers m and k, go from top to bottom.

As we have mentioned in the introduction, an important statistical quantity for an experimentalist studying chaotic transients is their average lifetime. Figure 7

https://doi.org/10.1017/S014338570000300X Published online by Cambridge University Press

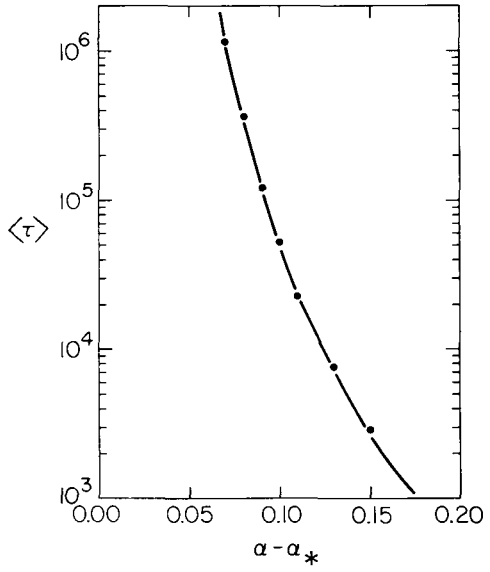

FIGURE 7. $\langle\tau\rangle$ versus $\alpha - \alpha_*$. Dots denote numerical results while solid line denotes theoretical result given by equation (15).

shows numerical (dots) and theoretical results for the average lifetime of chaotic transients for the map given by equations (1) as a function of the parameter α. The numerical results are obtained by averaging over 100 initial conditions in the former basin of attraction. The initial conditions were chosen randomly in $\theta_0 \in [0, 2\pi)$ with $z_0 = 0.0011$. The solid curve is obtained from the theoretical prediction, given by

$$\langle\tau\rangle = \kappa L_u^{\pi/a^{\frac{1}{2}}}. \tag{5}$$

for α slightly larger than α_*, where

$$a = \beta^{\frac{1}{2}}(\alpha - \alpha_*) + \left(\frac{\alpha - \alpha_*}{2}\right)^2, \tag{6}$$

L_u is 2, $\langle\tau\rangle$ is the average lifetime of a chaotic transient, and κ is a constant which is chosen to yield a good fit to the data. We note that the theoretical and numerical results agree very well.

A rigorous derivation of the right hand side of (5) is given in § 4. In fact we show the right-hand side is a lower bound for $\langle\tau\rangle$. This is appropriate since the dynamics elsewhere could increase the average lifetime further. Here it suffices to give an intuitive introduction to the ideas. To justify equation (5) we observe that for $\alpha > \alpha_*$, the two fixed points have already coalesced and, hence, there is an aperture around $\theta = 0$ through which the orbit can escape. Figure 8(a) shows the aperture of width l about $\theta = 0$ in which the orbit must enter to be ejected. The orbit needs to stay in the aperture long enough, say T iterates, to march up through the opening and exit the region $z < 2$. The orbit might fail to stay close to $\theta = 0$ because the θ direction is unstable with eigenvalue $L_u = 2$, pulling the orbit back into the chaotic remnant.

https://doi.org/10.1017/S014338570000300X Published online by Cambridge University Press

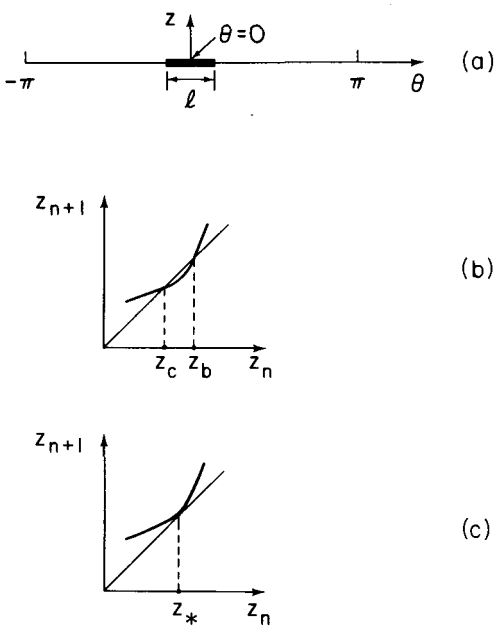

FIGURE 8. (a) State space (θ, z) showing the interval l about $\theta = 0$ inside which the orbit must fall to leave the chaotic attractor. (b) Local picture of z_{n+1} versus z_n of the z map for $\theta = 0$ and $\alpha < \alpha_*$. z_b and z_c are the unstable and stable fixed points, respectively. (c) Same as (b) but $\alpha > \alpha_*$. z_* is the z value at which z_b and z_c coalesce.

Thus, after T iterates the trajectory is within $L_u^T l$ of 0, and we need $L_u^T l < 1$ since otherwise $\cos\theta$ is not near $+1$. We estimate l as

$$l < \frac{\kappa_1}{L_u^T},$$

where κ_1 is a constant of the same order of magnitude as one. Almost any initial condition in θ will generate an orbit which yields a time asymptotic uniform distribution in θ. Thus the probability of θ_{n+1} falling in the interval $(-l/2\pi, l/2\pi)$ if θ_n is not in that interval is $l/2\pi$. Thus

$$\langle \tau \rangle = \frac{2\pi}{l} = \kappa L_u^T = \kappa\, e^{T \ln L_u}, \tag{7}$$

where $\kappa = 2\pi/\kappa_1$ is a constant.

Now, we need to evaluate T, the time it takes for the orbit to exit once it has fallen in the aperture. For α slightly greater than α_*, the aperture width is very small and we can then approximate θ by 0 and $\cos\theta$ by 1. In this case equation (1a) becomes

$$z_{n+1} = \alpha z_n + z_n^2 + \beta. \tag{8}$$

This is a quadratic equation with two fixed points z_c and z_b, for $\alpha < \alpha_*$ as shown in figure 8(b). For $\alpha > \alpha_* = 1 - 2\beta^{\frac{1}{2}}$, the fixed points do not exist. Figure 8(c) shows

https://doi.org/10.1017/S014338570000300X Published online by Cambridge University Press

the mapping (8) for $\alpha = \alpha_*$. Writing

$$z_{n+1} - z_n = (\alpha - 1)z_n + z_n^2 + \beta,$$

the minimum of the right-hand side occurs at

$$z_* = \frac{1-\alpha}{2}. \tag{9}$$

We rewrite equation (8) letting $\delta = z - z_*$,

$$\delta_{n+1} = \delta_n + \delta_n^2 + a, \tag{10}$$

where in this expression a is given by

$$a = \beta - \left(\frac{1-\alpha}{2}\right)^2. \tag{11}$$

At this point, we approximate the local quadratic map (10) by the following differential equation [9] for α near α_*,

$$\frac{d\delta}{d\tau} = \delta^2 + a. \tag{12}$$

The solution of equation (12) gives

$$T \approx \frac{1}{a^{\frac{1}{2}}} \int_{-\infty}^{\infty} \frac{d\zeta}{\zeta^2 + 1}.$$

This assumes $\zeta = \delta/a$ ranges from very negative values to very large positive values, which in turn means that the largest and smallest (most negative) values of δ have absolute value many times greater than $a^{\frac{1}{2}}$. Hence, the time for the orbit to exit the remnant once it has fallen in the aperture can be estimated as

$$T \approx \frac{\pi}{a^{\frac{1}{2}}}. \tag{13}$$

Substituting (13) into (7) we obtain

$$\langle \tau \rangle \approx \kappa L_u^{\pi/a^{\frac{1}{2}}}. \tag{14}$$

Using equation (4), the expression for a as given by equation (11) can be put in the form given by equation (6). Specializing to our parameters, $\beta = 0.04$ and $\alpha_* = 0.6$, we obtain

$$\ln \langle \tau \rangle \approx \frac{2.178}{\left[0.4\left(\frac{\alpha - 0.6}{2}\right) + \left(\frac{\alpha - 0.6}{2}\right)^2\right]^{\frac{1}{2}}} - 3.653, \tag{15}$$

where we have chosen $\ln \kappa = -3.653$ to give a good fit.

The coincidence of formula (15) with the numerical results shown in figure 7 is striking. As α approaches $\alpha_* = 0.6$, the width l decreases and it is more difficult for this trajectory to escape. In general, we expect to obtain lower bounds on how $\langle \tau \rangle \to \infty$ as $\alpha \to \alpha_*$. The extraordinary aspect of figure 7 is that the long chaotic transients associated with the unstable-unstable pair bifurcation can be extremely persistent as the parameter is varied. For instance, even at values of $\alpha \sim 20\%$ above α_*, i.e. $(\alpha - \alpha_*)/\alpha = 0.2$, the transient is of the order of 10^4 iterates, while for

$(\alpha - \alpha_*)/\alpha_* \sim 0.1$ we have $\langle\tau\rangle > 10^6$. Thus fine tuning of the experimental parameters is not required to encounter situations with long-lived chaotic transients. Another description of this persistence of long-lived chaotic transients for large values of $(\alpha - \alpha_*)/\alpha_*$ can be seen in the theoretical prediction for $\langle\tau\rangle$ given by equation (5). The decay rate, $1/\langle\tau\rangle$, can be thought of as the probability of being ejected from the region of the attractor remnant on a given iterate. Then the decay rate is zero at α_*, as it should be; but in addition, all derivatives $(d^n/d\alpha^n)(\langle\tau\rangle^{-1})$ are also zero at $\alpha = \alpha_*$. This means that $1/\langle\tau\rangle$ increases very slowly from zero as $(\alpha - \alpha_*)$ increases.

These results for the unstable-unstable pair bifurcation are to be contrasted with other known types of chaotic transients which also arise at a crisis. For instance, for the logistic map and for the Henon map, a typical result is $\langle\tau\rangle \sim (\alpha - \alpha_*)^{-\gamma}$, where $0 < \gamma < 1$ (cf. [**5**]), and long decay times only exist for $(\alpha - \alpha_*)/\alpha_*$ extremely small. For the Lorenz system using typical parameters where $\langle\tau\rangle \sim (\alpha - \alpha_*)^{-\nu}$ with ν approximately 4.0 (cf. [**10**]), so this transient is more persistent. The exponents γ and ν are called the *order of the crises.* The crisis we have been describing, which results in super persistent chaotic transient, has order ∞.

In this example, it might seem our result occur because the θ equation is non-invertible. In the next section, the θ equation is replaced by an invertible process on a torus. While the map in the next section is still not invertible, minor changes could be made that would make the map invertible. We prefer, however, to deal with examples for which computations are easy.

3. *Long-lived chaotic transients in a three-dimensional invertible map*

In this example we find that the chaotic attractor and the basin boundary are apparently fractal tori embedded in a three-dimensional space $\mathbb{R} \times T^2$. Before introducing the example, we wish to show how the unstable-unstable pair bifurcation occurs in a three-dimensional map. Figure 9 illustrates schematically how the two unstable fixed points, a repeller R and a saddle A, are created as a parameter δ decreases through one. The map in figure 9 may be written as

$$u_{n+1} = L_u u_n, \tag{16a}$$

$$s_{n+1} = L_s s_n, \tag{16b}$$

$$\xi_{n+1} = \xi_n + \xi_n^2 + \alpha, \tag{16c}$$

where $0 < L_s < 1 < L_u$. The two fixed points of this map have $\xi = \pm(-\alpha)^{\frac{1}{2}}$. At $\alpha = 0$, the Jacobian of the equation (16) at the unique fixed point has an eigenvalue $+1$, as is true whenever fixed points coincide. For maps with such bifurcations, a chaotic attractor can lie in the closure of the unstable manifold of the saddle corresponding to A. Similarly, time reversal changes the role of R and A, and the closure of the stable manifold of R can be a chaotic repeller which forms the basin boundary of the chaotic attractor. This appears to be the case in our example. When this is in fact true and the point A is in the chaotic attractor, then when A coalesces with R we expect a crisis which will destroy the chaotic attractor and its basin of attraction. By varying the parameter in the opposite direction, a chaotic attractor is born as in

https://doi.org/10.1017/S014338570000300X Published online by Cambridge University Press

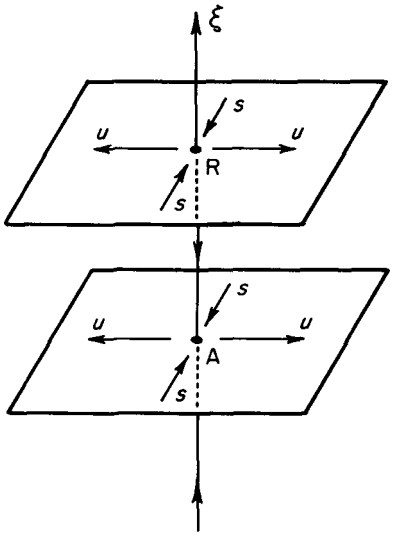

FIGURE 9. Schematic illustration of an unstable pair bifurcation in a three dimensional map. R is a repeller and A is a saddle.

the two-dimensional non-invertible map which we have discussed in the previous section.

The example [5] that we choose is a modification of the map given by equations (1):

$$\theta_{n+1} = \theta_n + \phi_n, \qquad \text{mod } 1, \tag{17a}$$

$$\phi_{n+1} = \theta_n + 2\phi_n, \qquad \text{mod } 1, \tag{17b}$$

$$z_{n+1} = \alpha z_n + z_n^2 + \beta \cos(2\pi\theta_n). \tag{17c}$$

We may think of θ and ϕ as angle coordinates and z as a radial coordinate, meaning that we are dealing with a toroidal coordinate system.

The map (17) has two unstable fixed points at $\theta = \phi = 0$,

$$z = z_{R,A} = \tfrac{1}{2}\{(1-\alpha) \pm [(1-\alpha)^2 - 4\beta]^{\frac{1}{2}}\},$$

corresponding to R and A of figure 9. The crisis occurs at $\alpha = \alpha_* = 1 - 2\beta^{\frac{1}{2}}$. Figure 10 shows a $\phi = 0$ cross-section of the attractor (inner curve). We use a polar coordinate representation for θ, z choosing $z - 0.1$ as the distance from the origin and $2\pi\theta$ as the angle from the vertical. The origin of the polar system is indicated by a dot. This figure is constructed by iterating the map (17), with $\beta = 0.04$ and $\alpha = 0.58 < \alpha_* = 0.60$, and plotting points whose ϕ values lie between $\phi = \pm 10^{-3}$. The basin boundary is the curve encircling the attractor. It is obtained similarly by iterating the inverse map (choosing the plus sign when inverting the quadratic z equation). The cross-section of both the chaotic attractor and the repeller appear to be fractal. Orbits with initial points at radial positions falling within the region bounded by the repeller are attracted to the chaotic attractor, while those starting outside this region asymptote to $z = +\infty$ as $n \to \infty$. Thus the repeller toroidal surface

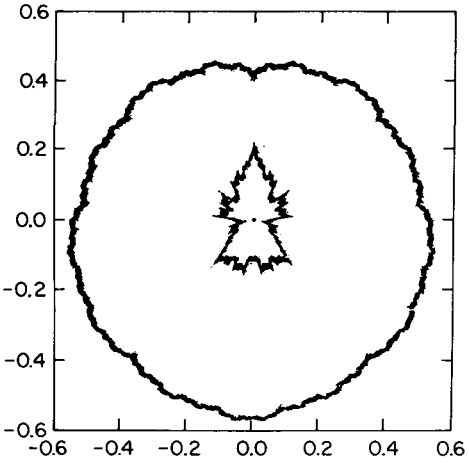

FIGURE 10. $\phi = 0$ cross-section of the toroidal attractor (inner curve) and its basin boundary (outer curve) for $\alpha = 0.58 < \alpha_*$ and $\varepsilon = 0.04$. The dot in the centre is the origin of the polar coordinate system of angle $2\pi\theta$ and radius $z - 0.1$.

is the boundary of the basin of attraction for the toroidal chaotic attractor that lies inside.

As the parameter α is raised, the z coordinates at $\theta = \phi = 0$ of the chaotic attractor and basin boundary move towards each other (as in the previous example) until they touch for $\alpha = \alpha_* = 0.60$. After the crisis occurs, the attractor and repeller remnants are still visible in our plots because the chaotic transients can be very long. Figure 11 shows a plot of the chaotic transient for $\beta = 0.04$ and $\alpha = 0.68 > \alpha_*$. We observe the apparent joining of the transient attractor and repeller at $\theta = 0$. For the parameters of figure 11, the length of the chaotic transient, averaged over the

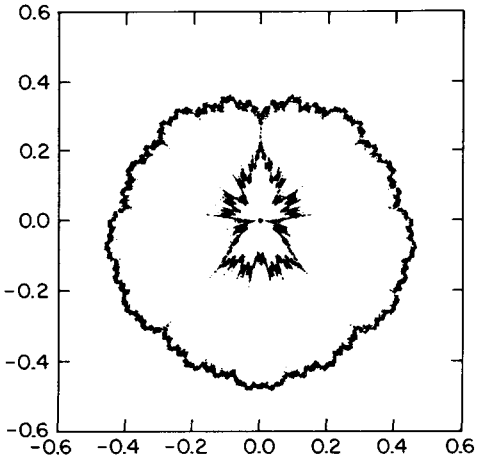

FIGURE 11. Picture of the remnants of the chaotic attractor and repeller obtained by iterating the map (17) for $\varepsilon = 0.04$ and $\alpha = 0.68 > a_* = 0.60$. It is plotted $2\pi\theta$ and $z - 0.1$.

https://doi.org/10.1017/S014338570000300X Published online by Cambridge University Press

initial conditions, is approximately 10^7 even though α substantially exceeds α_* since $(\alpha - \alpha_*)/\alpha_* = 0.12$. The connection joining the toroidal attractor and repeller in figure 11 is very thin. Thus we may think of the attractor as developing a hole. If the hole is small it takes a long time for an orbit to fall into it. This hole reflects the fact that trajectories can go to ∞ only after having $\cos\theta$ nearly 1 for several iterates in a row. This is possible only if θ and ϕ are near the origin.

To facilitate the evaluation of the average lifetime of the long-lived chaotic transient we change coordinates in the plane θ, ϕ by rotating the axes about the origin to an (η, ξ) system as shown in figure 12, where the η axis is the unstable

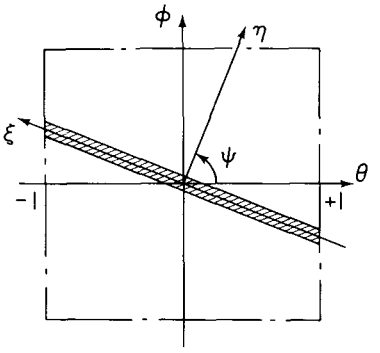

FIGURE 12. New system of coordinates (η, ξ) for the θ, ϕ part of the map (17). η is along the unstable direction and ξ along the stable. Trajectories about to diverge with $z \to \infty$ must lie in a narrow band about the ξ axis.

direction and the ξ axis is the stable direction in T^2. The unstable eigenvalue of equations (17a) and (17b) is

$$L_u = \frac{3+\sqrt{5}}{2} \tag{18}$$

and the stable eigenvalue is $L_s = 1/L_u$. Now an initial point (η_0, ξ_0) near $(0, 0)$ becomes $(\eta_0 L_u^{\tau}, \xi_0 L_u^{-\tau})$ after a time τ. Then, the probability of ejection per iterate of the map, i.e. the decay rate, of the transient is proportional to the area of the region near the origin where the hole is formed. Actually the hole is a tapered band about the ξ axis; the thickest part is near $(0, 0)$. Hence, the average lifetime is inversely proportional to the decay rate, or,

$$\langle \tau \rangle \approx \kappa L_u^{T}, \tag{19}$$

where T is the time it takes for the orbit to exit after it has reached the hole. Now, to estimate T, the calculation is the same as in the two-dimensional case since equation (1b) is the same as equation (17c). Equation (13) is now again valid with a in equation (6) or (11) unchanged, where for $\beta = 0.04$, $\alpha_* = 1 - 2\beta^{\frac{1}{2}} = 0.60$ and L_u is given in equation (18). Hence equation (14) again applies. Figure 13 shows a plot of $\langle \tau \rangle$ versus $\alpha - \alpha_*$ for $\beta = 0.04$ obtained from numerical iterations (dots) and from equations (14) and (18) (solid curve) with the parameter κ chosen to give a

https://doi.org/10.1017/S014338570000300X Published online by Cambridge University Press

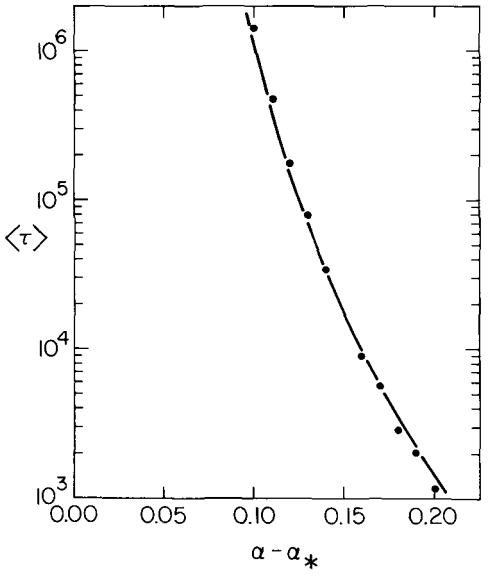

FIGURE 13. Chaotic transient average lifetime versus $\alpha - \alpha_*$ for equations (17) with $\varepsilon = 0.04$. The dots are experimental results while the solid line denotes result from equations (14) and (18) or $\ln\langle\tau\rangle = 3.024/[0.2(\alpha - 0.6) + (\alpha - 0.6)^2/4]^{\frac{1}{4}} - 6.221$, where we have chosen $\ln\kappa = -6.221$ to give a good fit.

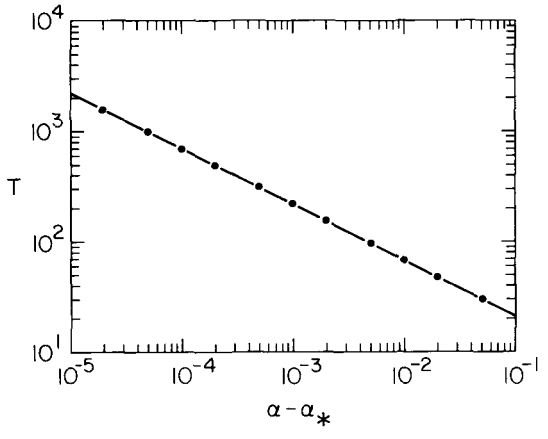

FIGURE 14. Plot of the time it takes for the orbit to exit when $\theta = \phi = 0$. The dots are experimental results while the straight line denotes result from (13), i.e. $T = \pi/[0.2(\alpha - 0.6) + (\alpha - 0.6)^2/4]^{\frac{1}{4}}$ for $\beta = 0.04$.

good fit. It is seen that equation (14) agrees well with the numerical experiments giving the observed behaviour, except that $\langle\tau\rangle$ increases even slightly faster than predicted as $\alpha \to \alpha_*$. Figure 14 shows formula (13) (solid line) and the experimental results (dots) for an orbit initialized at $\theta = \phi = 0$. In addition, we have verified numerically that for a random collection of initial points chosen from a uniform distribution of initial conditions in the formerly chaotic region, the lifetimes of the

https://doi.org/10.1017/S014338570000300X Published online by Cambridge University Press

chaotic transients are very nearly exponentially distributed, namely,

$$\chi(\tau) = \frac{1}{\langle\tau\rangle} \exp\left(-\tau/\langle\tau\rangle\right), \tag{20}$$

where $\chi(\tau)$ denotes the distribution of lifetimes, and $\langle\tau\rangle$ is the average lifetime.

We have also examined equations (17), but with the $\cos(2\pi\theta)$ term replaced by $\sin(2\pi\theta)$. Figure 15 shows a picture of the $\phi = 0$ cross-section of the attractor and

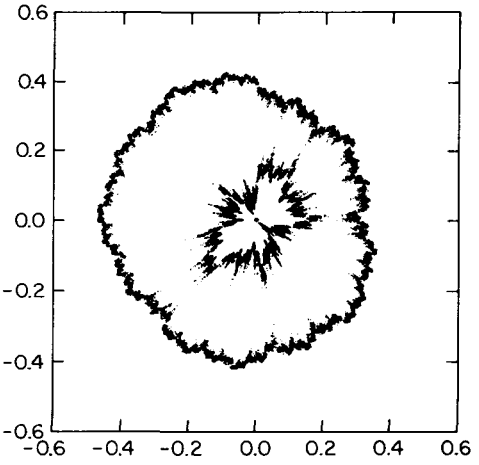

FIGURE 15. $\phi = 0$ cross-section of the attractor and its basin boundary for equations (17) but with $\cos(2\pi\theta_n)$ replaced by $\sin(2\pi\theta_n)$, $\beta = 0.04$, and $\alpha = 0.71$.

its basin boundary for such a case. In the sine case there is no *a priori* reason to think that as α is raised the attractor will be destroyed by a crisis (i.e. by a collision with a periodic orbit). We observe in a number of detailed numerical experiments, however, that the attractor appears to be destroyed when it and its basin boundary touch at the coalescence of two unstable period four orbits (one in the attractor and one in the basin boundary). The period four orbit in question has (θ, ϕ) coordinates given by $(\frac{2}{15}, \frac{1}{15}) \to (\frac{3}{15}, \frac{4}{15}) \to (\frac{7}{15}, \frac{11}{15}) \to (\frac{4}{15}, \frac{14}{15}) \to (\frac{2}{15}, \frac{1}{15})$. For this orbit in (θ, ϕ) space, the pair annihilation occurs at the value $\alpha = \alpha_* \approx 0.6618717$.

Figure 16 is the plot of the average lifetime of the chaotic transient versus $\alpha - \alpha_*$ for the map (17) where $\cos(2\pi\theta)$ is replaced by $\sin(2\pi\theta)$. The experimental results indicated by dots agree well with the solid curve $\ln\langle\tau\rangle = 5.71(\alpha - \alpha_*)^{-\frac{1}{2}} - 8.33$, where $\alpha_* = 0.6618717$. The constants were chosen to optimize the fit.

4. *The persistence of super-long transients despite perturbations*

We have exhibited rather special systems that have super-long transients. We also claim that such phenomena can be expected in nature. What we mean by this is that the phenomena we have presented can be expected to persist under perturbations. The difficulty faced in demonstrating this is that local behaviour (near the annihilation point) interacts with large scale dynamics throughout the region where

https://doi.org/10.1017/S014338570000300X Published online by Cambridge University Press

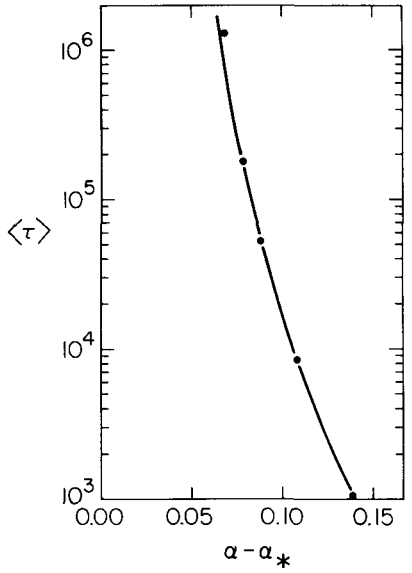

FIGURE 16. $\langle\tau\rangle$ versus $\alpha - \alpha_*$ for the map given by equations (17) with $\sin(2\pi\theta)$ instead of $\cos(2\pi\theta)$ in equation (17c). The dots indicate experimental results whereas the solid curve represents the curve $\ln\langle\tau\rangle = 2.425/[0.2(\alpha - \alpha_*) + (\alpha - \alpha_*)^2/4]^{\frac{1}{2}}$, where $\alpha_* = 0.6618717$ and the constants are chosen to give a good fit.

chaotic trajectories have been travelling. In our examples in the 'transient' regime, a tiny region B plays a special role, as shown in figure 17 at the instant of annihilation. This tiny region is centred at the point p_0 where the unstable-unstable pair annihilation bifurcation occurred. In this section we assume the pair annihilation occurs at $\alpha = \alpha_* = 0$.

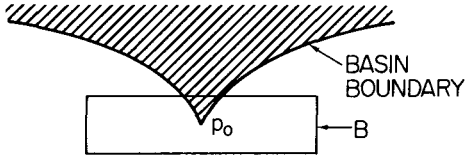

FIGURE 17. Sharp spike of the basin boundary ending in the box B at p_0.

For α slightly larger than 0, a typical trajectory wanders through the region where the attractor was and behaves just as before the annihilation. Eventually it enters the tiny region B and with high probability it soon leaves B and again wanders as before. After going through this process many times, it again enters B and now a low probability event occurs; namely, the trajectory departs through an extremely small window in a different direction, leaving the vicinity of the defunct attractor, never to return.

The formula describing the super long persistence of the chaotic attractor is in reality a statement that each time a typical trajectory enters B, it is extremely unlikely

https://doi.org/10.1017/S014338570000300X Published online by Cambridge University Press

(when the parameter is near the annihilation value) that the trajectory will escape vertically through the window. It is far more likely it will leave B through sides that lead to the old attractor region. As in previous sections we must show that when a trajectory exists via this window, it must typically have been in B a long time. We now summarize the local behaviour on which the formulae depend.

Local Behaviour. For values of the parameter α less than 0 there is a pair of periodic orbits, both of period k and both unstable. One is on the chaotic attractor and the other is on the attractor's basin boundary. At $\alpha = 0$ they collide and are destroyed. This annihilation is essentially the same as a saddle-node bifurcation for period k orbits except that in our case, both orbits are unstable. We assume that the basin boundary and the attractor meet at $\alpha = 0$ at only the k points where these orbits collide. We speak of an 'attractor' at $\alpha = 0$ even though it does not attract every point in a neighbourhood.

Without loss of generality we can assume the period k is 1, since otherwise we could examine the kth iterate of the map. Our proof could be adapted so that the basin boundary points collide with the attractor at k points simultaneously instead of just a single point.

Let p_0 denote the phase space point where the two orbits meet. This generalized pair annihilation can only occur when the Jacobian of the map at p_0 and $\alpha = 0$ has $+1$ as an eigenvalue, and we assume $+1$ is a *simple* eigenvalue and that the Jacobian has no other eigenvalues on the unit circle. We also assume there is at least one other eigenvalue outside the unit circle; see figure 18. This guarantees that neither orbit is stable for α near 0. We let L_u denote the largest absolute value of the eigenvalues. The centre manifold theorem says that since there is a unique eigenvalue of the map with absolute value 1, there is a two-dimensional manifold M_1 in p, α space containing the annihilation point $(p_0, 0)$ and the map carries points of M_1 to points of M_1, at least for points near p_0 with α near 0. (The centre manifold theorem is an existence theorem and, in fact, there are infinitely many ways of choosing M_1. In the case where all the eigenvalues of $DF(0, p_0)$ are >0, it contains the unique (non-constant) trajectory at $\alpha = 0$ that goes to p_0 as t goes to infinity. It must also contain *some* trajectory that goes to p_0 as t goes to $-\infty$, but this trajectory is not uniquely determined.) The centre manifold theorem says we can introduce a coordinate z (scalar) so that the dynamics on M_1 are given by

$$z_{n+1} = F(\alpha, z_n) \tag{21}$$

for an appropriate choice of the functions F for α near 0.

We assume the pair annihilation is generic: F_{zz} and F_α are not 0 at $(0, p_0)$. See [6] for the genericity equations for the case of general coordinates. Without loss of generality we can assume the coordinates are oriented so that at $(0, p_0)$,

$$\beta_0 = F_{zz} > 0, \tag{22}$$

and

$$a_0 = F_\alpha > 0. \tag{23}$$

https://doi.org/10.1017/S014338570000300X Published online by Cambridge University Press

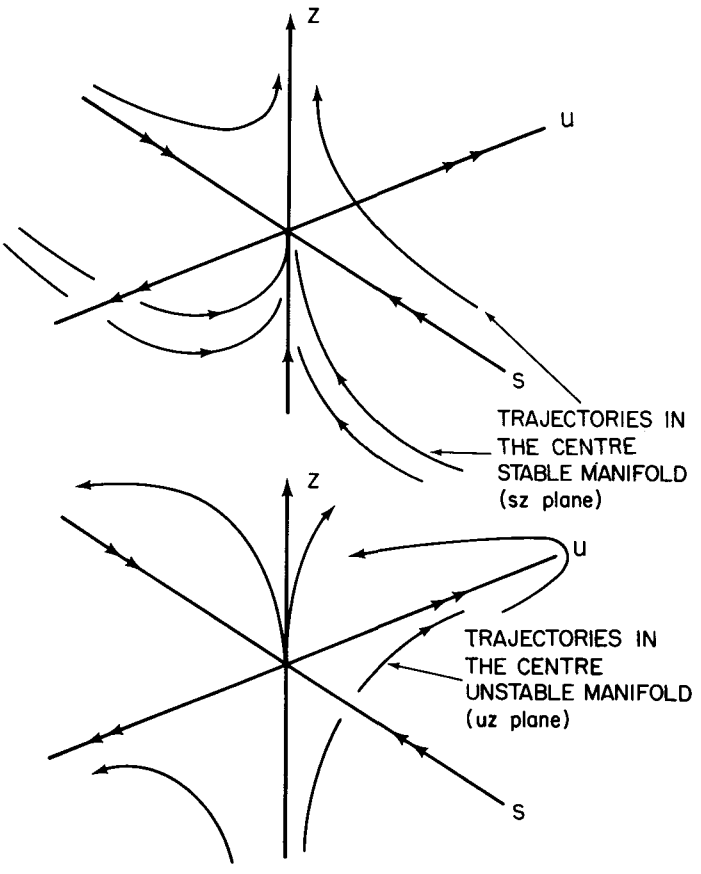

FIGURE 18. The two graphs show phase space at $\alpha = 0$. The vertical axis is the z axis, the points in the centre manifold having $\alpha = 0$. In (a) the trajectories shown are all in the centre-stable plane while in (b) they are in the centre-unstable plane.

When the system is perturbed slightly, that is, when the perturbation and all its first and second partial derivatives are sufficiently small, our 'local' hypotheses remain valid; there will still be an annihilation of a pair of periodic orbits (though the value $\alpha = 0$ at which it occurs may be changed slightly) and the bifurcation will be generic as described above. Furthermore, as we will argue below, the collision between the orbits still occurs at a point that is on the boundary of the basin. Therefore to prove that super-long transients can be expected in nature, it is sufficient to prove that they occur whenever the hypotheses under discussion are satisfied. There is, however, a difficulty: there are no very general hypotheses that guarantee the existence of chaotic attractors. It is therefore necessary that we state our results as local results, estimating *how many times a trajectory can be expected to re-enter B* before finally escaping through the top.

Let B denote a small box centred at p_0, as shown in figures 19(a) and 19(b). Let C be a curve in phase space that runs through the box and while in the box it is

https://doi.org/10.1017/S014338570000300X Published online by Cambridge University Press

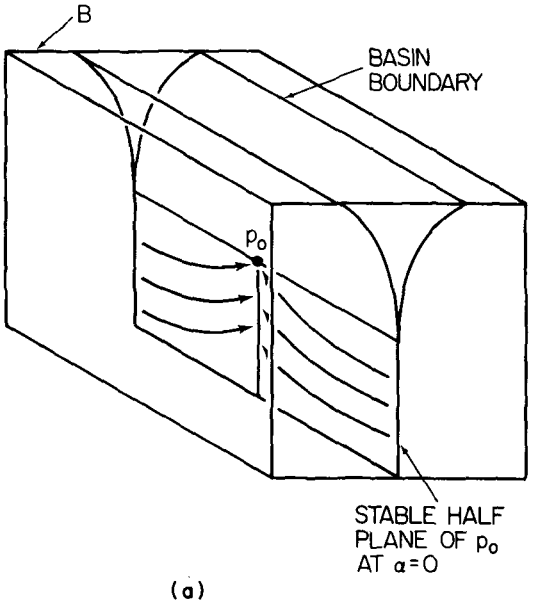

(a)

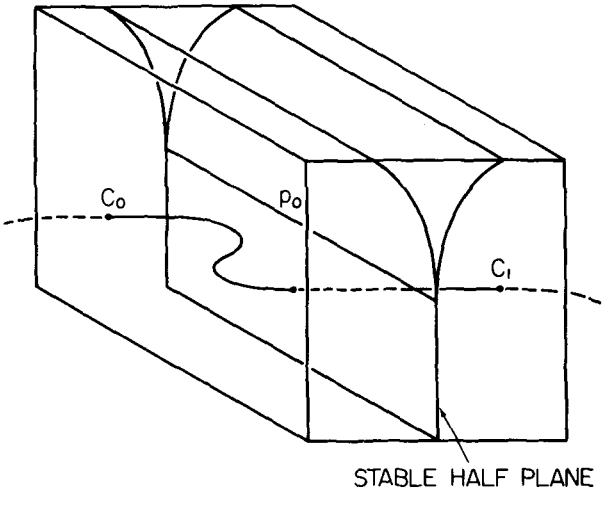

(b)

FIGURE 19. The curves in figure 18(a) that tend to p_0 at $\alpha = 0$ constitute what we call the 'stable half plane' and it is redrawn in (a). The basin boundary is the wedge cutting into B from above. Imagine a curve in B that is about to leave B on the next iterate. As it then is mapped for many iterates its image is stretched greatly and then finally part of the image of the n'th iterate of the curve re-enters the box, and that n'th image is called C_0C_1. In (b) the curve C_0C_1 enters the box B at C_0 and exits at C_1. (c) shows the same picture where there is no stable direction. For α slightly greater than 0 we ask how much of the segment $\Gamma_0\Gamma_1$ leaves B through the boundary of B at the top of the wedge since such points will never return to B. That is, how long is the segment D_0D_1 shown in (d). Notice that when $\alpha > 0$ the wedge immediately slices all the way to the bottom of B and the walls of the wedge should be considered much closer together than it is possible to show here.

https://doi.org/10.1017/S014338570000300X Published online by Cambridge University Press

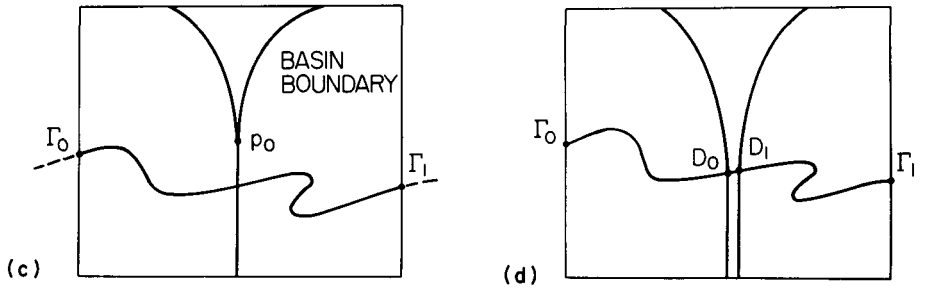

FIGURE 19 (*cont.*)

in the basin when $\alpha = 0$. It does not touch the basin boundary. We require that C is chosen so as to pass once through M_s, the stable half manifold of p_0, and we assume it is not tangent to M_s at the point where they touch. For a point p chosen at random on C and in B, the trajectory will eventually leave the box (with probability 1). Let P_α be the probability that the trajectory escapes some neighbourhood of the old attractor and never returns to the box. Such points will be called *wayward*, assuming the point is chosen at random from the curve with the probability of choosing it in a given segment being proportional to the segment's length. Of course, $P_\alpha = 0$ for $\alpha < 0$. We claim:

THEOREM. *Let* $Q = \alpha a_0 \beta_0$. *Then*

$$P_\alpha L_u^{\pi/Q^{\frac{1}{2}}} \to 0 \qquad \text{as } \alpha \to 0^+. \tag{24}$$

When the unstable manifold has dimension greater than 1, L_u can then be replaced by the absolute value of the product of the 'expanding' eigenvalues; that is, of the eigenvalues having absolute value greater than one. The theorem implies that P_α is bounded above by a function $L_u^{\text{const.}\alpha^{-\frac{1}{2}}}$ that has derivatives of all order equal to 0 at $\alpha = 0$. The average length $\langle \tau \rangle$ of the transient, $1/P_\alpha$, may then be said to be 'super-long' since for any $k > 0$, $1/P_\alpha > 1/\alpha^k$ for $\alpha > 0$ sufficiently small. Equation (24) differs from (5) and (14) in that we now obtain a lower bound for $\langle \tau \rangle$, that is, $\langle \tau \rangle \geq \kappa L_u^{\pi/Q^{\frac{1}{2}}}$ and this is valid for any κ provided α is small enough.

In the remainder of this section we will first prove this result in the two dimensional case appropriate for non-invertible maps (figures 19(c) and 19(d)) as in the example in § 2. Then the required changes are discussed to make the proof general, allowing the unstable manifold at the annihilation pair to be multidimensional and permitting the annihilation pair to have a stable manifold.

To coordinatize the space we introduce a coordinate u which is 0 on M_1. Then for an appropriately chosen function G and an appropriate definition of F off M_1, the dynamics are given by

$$z_{n+1} = F(\alpha, u_n, z_n), \tag{25a}$$

$$u_{n+1} = G(\alpha, u_n, z_n). \tag{25b}$$

F was already defined on M_1 (i.e. where u is 0) so the old function $F(\alpha, z)$ is now $F(\alpha, 0, z)$. G is chosen so that it is 0 on M_1, i.e. $G(\alpha, 0, z) \equiv 0$. From now on we can denote p_0 by $(0, 0)$ in u, z coordinates. The z coordinate can be chosen so that

https://doi.org/10.1017/S014338570000300X Published online by Cambridge University Press

the curve where $\alpha = 0$ and $z = 0$ is the unstable manifold M_u of p_0. Of course, M_u is invariant under the map. This may be restated as follows:

$$F(0, u, 0) = 0.$$

Our assumption that the pair annihilation is generic now permits a conclusion about the shape of the boundary near p_0 for $\alpha = 0$.

PROPOSITION 1. *At $\alpha = 0$ the basin boundary is an exponentially sharp spike ending at p_0. (See figure 17.)*

The precise formulation of sharpness will become clear with the proof.

The proof of the main result depends on the dynamics near the pair annihilation. Thus we now restrict attention to a box $B = \{(\alpha, u, z)\}$ such that $0 \leq \alpha \leq \alpha_B$, $|u| \leq u_B$, $|z| \leq z_B$, where these bounding constants α_B, u_B, and z_B must be chosen sufficiently small. To begin with, they must be chosen small enough that there is a constant $L_B > 1$ such that in B,

$$|G(\alpha, u, z)| \geq L_B|u|.$$

By choosing the box small enough, L_B can be made as close to L_u as we wish.

Imagine a set W in u, z space that is a neighbourhood of the closure of the attractor's basin when $\alpha = 0$, and assume that for $\alpha = 0$, some trajectories starting arbitrarily close to $(0, 0)$ can escape from this neighbourhood. See figure 20. We

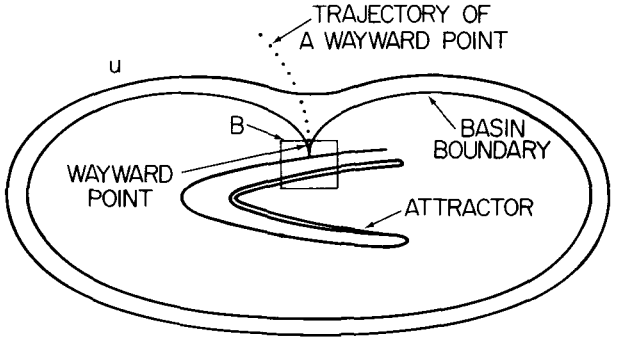

FIGURE 20. When $\alpha = 0$, W is a neighbourhood of the closure of the basin of the attractor.

are especially interested in trajectories for $\alpha > 0$ that leave B and never return. A point (α, u, z) of B is then wayward if the trajectory starting there leaves B and then leaves this neighbourhood W without ever returning to B. Our estimates work for any choice of W.

Assume the trajectory through $(\alpha, u_1, z_1) \in B$ eventually leaves B. We say the trajectory *exits through the top of B* if

$$|u_N| \leq u_B \quad \text{and} \quad z_N \geq z_B \tag{26}$$

for the first N for which (α, u_N, z_N) is not in the interior of B.

Claim. There is a choice of u_B, z_B, α_B (>0) such that every wayward point in B exits through the top of B.

https://doi.org/10.1017/S014338570000300X Published online by Cambridge University Press

The box is constructed by choosing points p_1 and p_2 in M_u at $\alpha = 0$, one on each side of 0, as shown in figure 21. We let S be the two segments of M_u (one on each side of 0) that have p_1, p_2 and their image points (q_1, q_2) as their end points. We may assume $|q_1| = |q_2|$. Let V be a neighbourhood of these segments with the closure of V lying in the interior of the basin of the attractor. We choose $u_B = |q_1| = |q_2|$.

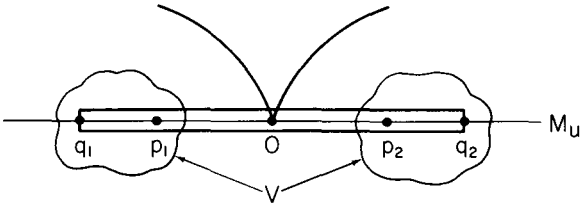

FIGURE 21. Points p_1 and p_2 in M_u at $\alpha = 0$ have points q_1 and q_2, respectively, as their images.

Then for z_B sufficiently small, the claim will hold since the basin boundary will then only meet B as shown in figure 17. We now require inequalities for proving both the proposition and the theorem.

Dynamic inequalities in B. For any choice of

$$a_B > a = (\partial/\partial\alpha)F \qquad \text{at } (0, 0, 0),$$
$$\beta_B > \beta_0 = \partial^2 F/\partial z^2 \qquad \text{at } (0, 0, 0),$$
$$\gamma_B > \gamma_0 = |\partial^2 F/\partial u\, \partial z| \qquad \text{at } (0, 0, 0),$$

we have

$$F(\alpha, u, z) \leq z + a_B\alpha + \gamma_B|uz| + \beta_B z^2, \tag{27}$$

when $(\alpha, u, z) \in B$, provided B is small enough; that is, provided α_B, u_B, z_B are small enough. This is true since $F(0, u, 0) \equiv 0$ and at $(0, 0, 0)$ we have $\partial F/\partial z = 1$. Similarly, if $L_B < L_u \equiv |\partial F/\partial u|$ at $(0, 0, 0)$ we have, for B small enough,

$$|G(\alpha, u, z)| \geq L_B u \qquad \text{in } B. \tag{28}$$

For any choice of B, we can assume a_B, β_B, γ_B, L_B are values for which (27) and (28) hold (and $L_B > 1$). They can be chosen as functions of B so that $a_B \to a$ and $\beta_B \to \beta$ and $\gamma_B \to \gamma$, and $L_B \to L$ as $\alpha_B, u_B, z_B \to 0$.

Equivalently, we may write (27) and (28) as

$$z_{n+1} - z_n \leq a_B\alpha + \gamma_B|u_n z_n| + \beta_B z_n^2, \tag{29}$$
$$|u_{n+1}| \geq L_B|u_n| \tag{30}$$

for any trajectory as long as $(\alpha, u_n, z_n) \in B$.

To prove proposition 1, let $(\alpha, u_0, z_0) \in B$ be a trajectory that exits through the top of B at $n = N$ with $\alpha = 0$. Notice $z_0 > 0$. Then, inequalities (29) and (30) are satisfied and

$$\left|\frac{u_n}{u_N}\right| \leq L_B^{-(N-n)} \qquad \text{for } 0 \leq n \leq N. \tag{31}$$

https://doi.org/10.1017/S014338570000300X Published online by Cambridge University Press

For $\alpha = 0$ it follows that for a small box $|z| \ll z_B$, we have $|z_{n+1}/z_n| \ll |u_{n+1}/u_n|$. Since $|z_N/u_N| \geq z_B/u_B$, the same must be true for earlier iterates. Therefore, $z_n/u_n \geq z_N/u_N$ for $n < N$, and $\gamma_B|u_n z_n| \leq \bar{\gamma} z_n^2$, where $\bar{\gamma} = \gamma_B u_B/z_B$. In (29) we set $\alpha = 0$ and obtain $z_{n+1} - z_n \leq \text{const.}\ z_n^2$ for trajectories that exit through the top of B. For simplicity we take const. $= 1$. We convert the inequality to a differential inequality with n a continuous variable (see remark below) so that

$$\frac{dz}{dn} \leq z^2 \tag{32}$$

$$\begin{aligned}
&\Rightarrow \int_{z_n}^{z_N} \frac{dz}{z^2} \leq N - n \\
&\Rightarrow z_n^{-1} - z_N^{-1} \leq N - n \\
&\Rightarrow \left|\frac{u_0}{u_N}\right| \leq L_B^{z_N^{-1} - z_0^{-1}} \qquad \text{[from (31)]} \\
&\Rightarrow |u_0| \leq u_B L_B^{(z_B^{-1} - z_0^{-1})} \qquad \text{[from (26)].}
\end{aligned} \tag{33}$$

The region bounded below by $u(z) = u_B L_B^{(z_B^{-1} - z^{-1})}$ might be called *exponentially sharp*, and all wayward points u, z lie in it since wayward points exit through the top of B. The proposition is proved.

We have cavalierly replaced a differential inequality by (32) even though they are not equivalent. However, they can be made close by choosing z_B small. In order to keep arguments intuitive, we will leave it to the reader to make fine tuning adjustments between difference and differential inequalities. Hence the correct form of (33), *based on arguments that the two types of inequalities are close*, is

$$|u_0| < \text{const.}\ L_B^{-1/z_0},$$

where the constant can be made as close to $u_B L_B^{1/z_B}$ as desired by choosing z_B small. In our case, however, (33) is actually correct since this differential inequality has solutions that increase slightly faster than any solutions of the difference equation (a result analogous to the benefits of instantaneous compounding of interest).

To see what can be achieved when no γ_B term is present in (27), we establish the following result. Assume $a_0 > 0$, $\beta_0 > 0$, and

$$z_{n+1} - z_n \leq a_0 \alpha + \beta_0 z_n^2 \qquad \text{for } 0 \leq n \leq N-1, \tag{34}$$

Also assume $\varepsilon > 0$ is sufficiently small and $R > 0$ is sufficiently large that

$$\tan^{-1}(R) > \pi\left(\frac{1-\varepsilon}{2}\right) \qquad \text{for } z_B > Rr_0 \quad \text{and} \quad z_0 < -Rr_0, \text{ where } r_0 = \left(\frac{\alpha_0 a_0}{\beta_0}\right)^{\frac{1}{2}}. \tag{35}$$

We then have the following.

LEMMA 1. *For α sufficiently small ($\alpha \leq \alpha_0$ for some α_0) the number of iterates T required using* (34) *for z to go from $-Rr_0$ to $+Rr_0$ satisfies*

$$T \geq \pi(1-\varepsilon)/Q_0^{\frac{1}{2}}, \qquad \textit{where } Q_0 = \alpha_0 a_0 \beta_0.$$

https://doi.org/10.1017/S014338570000300X Published online by Cambridge University Press

Proof. Since $a\alpha + \beta z_n^2$ is small compared with Rr_0 (or rather $a\alpha + (Rr_0)^2$ is small), when α is small, we convert to a differential inequality:

$$\frac{dz}{dn} \leq a_0\alpha_0 + \beta_0 z^2. \tag{36}$$

While (34) and (35) are not equivalent, the difference between them is small and decreases as α decreases. We now have

$$\int_{z_0}^{z_T} \frac{dz}{a_0\alpha_0 + \beta_0 z^2} \leq T.$$

Letting $s = z/r_0$, $s_0 = z_0/r_0 < -R$ and $s_T = z_T/r_0 > R$, we obtain

$$\int_{-R}^{R} \frac{r_0\, ds}{1+s^2} \leq a_0\alpha_0 T \Rightarrow \pi(1-\varepsilon) < \tan^{-1}(R) - \tan^{-1}(-R) \leq TQ_0^{\frac{1}{2}},$$

and the result is established.

By making B small, this can be made as close to L_u as desired. To make this precise and allow $\gamma_B \neq 0$, it is necessary to introduce a small box S within B.

A small box S within the big box B. Next we examine a small rectangle S in B defined by $0 \leq \alpha \leq \alpha_S$, $|u| \leq u_S$, $|z| \leq z_S$ with $0 < \alpha_S < \alpha_B$, $0 < u_S < u_B$, $0 < z_S < z_B$. We require the rectangle to be chosen so that trajectories that exit through the top of B will exit through the top of S (assuming $z_0 \leq z_S$). At $\alpha = 0$, it is sufficient to have

$$u_S > u_B L_B^{z_B^{-1} - z_S^{-1}}, \tag{37}$$

and then there will be an α_S such that our requirement is met. In our discussions from now on, this will be assumed to be true.

We will place a number of additional requirements on S. First we assume

(S_1) S contains none of the points of $\Gamma_0\Gamma_1$.

See figures 19(c) and 19(d).

Just as we chose a_B, γ_B, β_B, and L_B we now choose a_S, γ_S, β_S as small as possible and L_S as large as possible so that

$$F(\alpha, u, z) \leq z + a_S\alpha + \gamma_S|uz| + \beta_S z^2, \tag{38}$$

$$G(\alpha, u, z) \geq L_S|u|, \tag{39}$$

for $(\alpha, u, z) \in S$.

LEMMA 2. *For any small $\varepsilon_0 > 0$, the box S may be chosen so that when $\alpha \leq \alpha_S$, any trajectory exiting through the top of B also exits through the top of box S, and while the trajectory is in S,*

$$z_{n+1} - z_n \leq (1+\varepsilon_0)(a_0\alpha + \beta_0 z_n^2). \tag{40}$$

In other words the γ_S term may be replaced by introducing ε_0, which also permits the use of a_0 and β_0 instead of a_S and β_S. To prove this result we require S small enough that

(S_2) $a_S \leq (1+\varepsilon_0/3)a_0$ and $\beta_S < (1+\varepsilon_0/3)\beta_0$;

(S_3) $3\beta_S z_S \leq \log L_S$ (i.e. z_S is small);

(S_4) $\frac{1}{3}\varepsilon_0\beta_S z_S > 2\gamma_S u_S$ (i.e. u_S is small).

https://doi.org/10.1017/S014338570000300X Published online by Cambridge University Press

From (38) we have

$$z_{n+1} - z_n \leq a_S\alpha + \gamma_S|u_n z_n| + \beta_S z_n^2. \tag{41}$$

At the top of S where $z_n = z_S$, we can assume that α_S is small enough that the last term on the right side of (41) is the dominant term in that

$$\beta_S z_n^2 \geq a_S\alpha, \qquad \text{for } \alpha \leq \alpha_S, \tag{42}$$

$$\tfrac{1}{3}\varepsilon_0\beta_S z_n > \gamma_S|u_n| \qquad \text{(from } (S_4)\text{)} \tag{43}$$

and (42) remains true so long as

$$z_S \geq z_n \geq (a_S\alpha/\beta_S)^{\frac{1}{2}}. \tag{44}$$

We convert (41) to a differential inequality and invoke (42) and (43)

$$\frac{dz}{dn} \leq (2+\varepsilon_0/3)\beta_S z^2, \tag{45}$$

which holds as long as (42) and (43) are true. Rewriting (42) yields

$$z_S \geq z \geq (a_S\alpha/\beta_S)^{\frac{1}{2}}. \tag{46}$$

We claim (43) *holds for z in the range* (46). Suppose equality holds in (43) at $z = z_*$. This means that $z/|u|$ is larger than at z_* for $z > z_*$ so $\log(z)$ is growing at least as fast as $\log(u)$ at z_*. Then writing (42) and (43) in differential inequality form (evaluating at $z = z_*$)

$$\frac{d}{dn}\log(u) = \frac{1}{u}\frac{du}{dn} \geq \log(L_S) \geq 3\beta_S z_S \qquad \text{(from } (S_3)\text{)}$$

$$3\beta_S z_S > (2+\varepsilon_0/3)\beta_S z \geq \frac{1}{z}\frac{dz}{dn} = \frac{d}{dn}\log(z),$$

using (S_3), and then (45). This contradicts our prior conclusion on growth rates z_*. Hence no such z_* exists in the range (42) and the claim is proved.

Below this range we claim $a_S\alpha$ dominates γuz. Applying (43) to (41) in the range (44) gives

$$\begin{aligned} z_{n+1} - z_n &\leq a_S\alpha + (1+\varepsilon_0/3)\beta_S z_n^2 \\ &\leq (1+\varepsilon_0/3)(a_S\alpha + \beta_S z_n^2). \end{aligned} \tag{47}$$

At the bottom of range (44), $\beta z_n^2 = a_S\alpha$ so

$$\tfrac{1}{3}\varepsilon_0\alpha a_S > \gamma|u_n|z_n = \gamma|u_n z_n|. \tag{48}$$

Using arguments as above this can be seen to be true while

$$(a_S\alpha/\beta_S)^{\frac{1}{2}} \geq z_n \geq -z_S, \tag{49}$$

since $\log|u_n|$ increases faster than $\log|z_n|$ as n increases so $\gamma|u_n z_n|$ increases with n. In other words, $|u_n z_n|$ assumes its largest value in range (49) at the top of that range. Hence in range (49)

$$z_{n+1} - z_n \leq (1+\varepsilon_0/3)a_S\alpha + \beta_S z_n^2,$$

which implies (47). Hence (47) is true as long as z_n is in S. Now using (S_2) and (47) yields

$$z_{n+1} - z_n \leq (1+\varepsilon_0/3)^2(a_0\alpha + \beta_S z_n^2),$$

which in turn implies (40) and lemma 2 is proved.

https://doi.org/10.1017/S014338570000300X Published online by Cambridge University Press

PROPOSITION 2. *For any $\varepsilon > 0$ there is an $\alpha_S > 0$ such that if (u_0, z_0) is a wayward point on the curve $\Gamma_0\Gamma_1$, with $0 < \alpha \le \alpha_S$, then the trajectory (u_n, z_n) will remain in B for at least $(1-\varepsilon)\pi/Q^{\frac{1}{2}}$ iterates during which*

$$|u_{n+1}| \ge (1-\varepsilon) L_u |u_n|.$$

To prove proposition 2 we require that S is chosen so that

$$(S_5) \quad \arctan(z_S/r_S) > \frac{\pi}{2}(1-\varepsilon_1),$$

where $r_S = (\alpha_S a_S/\beta_S)^{\frac{1}{2}}$, ε_1 is a small number that we will discuss later. In other words, $z_S^2 \gg \alpha_S$. Converting (40) to an integral inequality

$$\int_{-z_S}^{z_S} \frac{dz}{a_S\alpha + \beta_S z^2} \le (1+\varepsilon_0) T,$$

where T is the minimum number of iterates that are needed for z_n to traverse the box S from bottom to top. Then as in lemma 1, letting $Q_S = \alpha_S a_S/\beta_S$,

$$\frac{\pi(1-\varepsilon_1)}{Q_S^{\frac{1}{2}}} < \frac{1}{Q^{\frac{1}{2}}}[\arctan(z_S/r_S) - \arctan(-z_S/r_S)] \le (1-\varepsilon_0) T$$

$$\Rightarrow T \ge \frac{\pi}{Q_S^{\frac{1}{2}}} \frac{1-\varepsilon_1}{2+\varepsilon_0} = \frac{\pi}{Q^{\frac{1}{2}}}(1-\varepsilon),$$

where $\varepsilon_S = Q_S/Q - 1$. Of course, ε_S can be chosen as small as desired by making S small. Hence we can make

$$\varepsilon = 1 - \left(\frac{Q}{Q_S}\right)^{\frac{1}{2}} \left(\frac{1-\varepsilon_1}{1+\varepsilon_0}\right)$$

as small as desired, so proposition 2 is valid.

To prove the theorem. Let P_α denote the fraction of the points on $\Gamma_1\Gamma_1$ that are wayward. Then P_α is no greater than the fraction that remains in B for $(1-\varepsilon)\pi/Q$ iterates. The u coordinate of every wayward point on $\Gamma_0\Gamma_1$ satisfies

$$|u_0| \le u_S[L_u(1-\varepsilon)]^{-(1-\varepsilon)\pi/Q^{\frac{1}{2}}}. \tag{50}$$

Notice that ε and u_S can be made as small as desired by choosing α small, and that $(1-\varepsilon)^{(1-\varepsilon)} < 1$. For $\alpha > 0$, let $L(\alpha)$ be the largest value of $L_u(1-\varepsilon)^{(1-\varepsilon)}$ for which (50) is true and S can be chosen as we have required above. The slope of $\Gamma_0\Gamma_1$ is finite when it crosses $u = 0$ (since it is transverse to M_0 at $\alpha = 0$), so P_α is at most a constant times the right-hand side of (50). Since $u_S \to 0$ as $\alpha \to 0$ there is a function $\kappa(\alpha)$ with $\kappa(\alpha) \to 0$ as $\alpha \to 0$ such that

$$P_\alpha < \kappa(\alpha) L(\alpha)^{-\pi/Q^{\frac{1}{2}}}.$$

Hence, $P_\alpha L(a)^{\pi/Q^{\frac{1}{2}}} \to 0$ as $\alpha \to 0$. *The theorem has now been proved in the case where there is no stable manifold.*

When there is a stable manifold, we introduce an additional coordinate v so that (i) at $\alpha = 0$, $v = 0$ for points of the unstable manifold of $(0, 0, 0)$, (ii) $u = 0$ for points of the stable manifold, and (iii) $z = 0$ on both manifolds. We may choose these coordinates so that for any α small $u = 0$ (and $v = 0$) are invariant surfaces. The

https://doi.org/10.1017/S014338570000300X Published online by Cambridge University Press

dynamics satisfy a more general version of inequalities (29), (30)

$$z_{n+1} \leq z_n + a_B\alpha + \gamma_B|u_n z_n| + \gamma'_B|v_n z_n| + \gamma''_B|u_n v_n| + \beta_B z_n^2,$$
$$|u_{n+1}| \geq L_B|u_n|,$$
$$|v_{n+1}| \leq L'_B|v_n|,$$

where $L_B > 1$ and $L'_B < 1$. Notice, however, that we need a new term γ''_B since there is no obvious way to choose coordinates so that $\alpha = 0$ and $z_n = 0$ imply $z_{n+1} \leq 0$. We can guarantee this only when $u_n = 0$ or $v_n = 0$.

Proving the theorem is now essentially equivalent to extending lemma 2 to this more general case. The proof that γ_S is small (in the sense of lemma 2) needs essentially no change from the arguments above. That γ' is small is argued analogously except that $\beta_B z_n^2$ dominates $\gamma_S|vz|$ in S when z is near $-z_S$ instead of $+z_S$. The term γ''_B however introduces new aspects. The new term $\gamma''_B|u_n v_n|$ is always small and so it poses only a small problem for appropriate choice of S. Choose $L_S > 1$ so that

$$|u_{n+1}| \geq L_S|u_n| \quad \text{and} \quad |v_{n+1}| \leq |v_n|/L_S.$$

If a trajectory is in S for T iterates, say for $n = 0, \ldots, T$, we have $|u_T| \leq u_S$ so that at an earlier time n, the rapid growth of u implies

$$|u_n| \leq u_S/L_S^{T-n}.$$

Furthermore, letting v_S denote the maximum of $|v|$ in S, $|v_0| \leq v_S$ so the rapid shrinking of v implies $|v_n| \leq v_S/L_S^n$. These inequalities taken together imply

$$|u_n v_n| \leq u_S v_S/L_S^T \qquad \text{for all } n.$$

For α small, it is clear that T is large. (Our difficulty has not been to show that T is large but rather that T satisfies specific inequalities). Hence, $|u_n v_n|$ can be made uniformly small for all wayward trajectories by choosing α small and is dominated by

$$a_S\alpha + \beta_S z_n^2.$$

The proof then proceeds as before.

5. *Effect of noise on long-lived chaotic transients*

It might be objected that the phenomena described in this paper may not occur in experiments because noise would be present in real systems. For the examples discussed in §§ 2, 3, we have numerically determined, however, that the addition of noise exacerbates the situation, making the transients even longer (in the sense to be defined below).

The following heuristic argument suggests why the chaotic transients are longer in the presence of noise. We expect that the effect of adding noise (a random perturbation added on each step of the map) to the two-shift map equation (1a) or the map equations (17a) and (17b) makes it a bit more difficult for a trajectory to remain near $\theta = \phi = 0$ (where cos is large). Of course, for improbable choices of the random θ and ϕ perturbations, it is still possible for the trajectory to escape.

https://doi.org/10.1017/S014338570000300X Published online by Cambridge University Press

By contrast, the effect of noise in the z map, either in equation (1b) or in equation (17c) is very significant. These equations in the presence of noise can be written as

$$z_{n+1} = \alpha z_n + z_n^2 + \beta \cos\theta + \gamma r_n, \tag{51}$$

where $\gamma > 0$ measures the noise level and $\{r_n\}$ is a random sequence with some probability distribution, with $\{r_n\}$ assuming values in $[-1, 1]$. Thus, we are considering *bounded* noise (i.e. $|\gamma r_n| \leq \gamma$). With bounded noise we define α_* to be that value of α below which almost all initial conditions do not generate orbits which go to $z = +\infty$. To obtain α_* we set $r_n = +1$ in (51) and solve for the coalescence of the fixed points. We obtain

$$\alpha_* = 1 - 2(\beta + \gamma)^{\frac{1}{2}} \tag{52}$$

instead of equation (4). For $\alpha > \alpha_*$ trajectories will eventually escape to $z = +\infty$ for almost every initial point and almost every sequence $\{r_n\}$. In order to make a comparison with the noiseless case of § 2 we keep the crisis value of the parameter $\alpha_* = 0.6$ fixed, i.e. $\beta + \gamma = (1 - \alpha_*)^2/4$, or, $\beta + \gamma = 0.04$. Figure 22 shows a plot of the average lifetime $\langle\tau\rangle$ versus $\alpha - \alpha_*$ for $\beta = 0.02$ and $\gamma = 0.02$. We should contrast

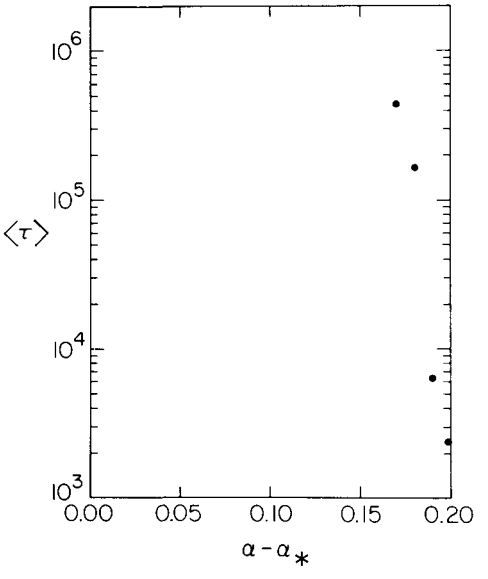

FIGURE 22. Plot of the average lifetime $\langle\tau\rangle$ versus $\alpha - \alpha_*$. The dots denote numerical results from equations (1a) and (51) for $\beta = 0.02$ and $\gamma = 0.02$. Contrast with figure 7.

these numerical results with the noiseless case shown in figure 7. The average escape time $\langle\tau\rangle$ is indeed much longer in the presence of noise. To understand this numerical observation we note that for $\alpha > \alpha_*$, in order for the orbit to leave, the term $\beta \cos\theta + \gamma r$ must be very close to its maximum, i.e. $\beta + \gamma = 0.04$ for many consecutive iterates. For that to happen, $\cos\theta$ and r must be close to $+1$. The $\cos\theta$ term has the same behaviour as in the noiseless case. But here we need in addition the randomly chosen noise to be close to $+1$ during the same sequence of iterates and

https://doi.org/10.1017/S014338570000300X Published online by Cambridge University Press

for many consecutive iterates. A formula analogous to (14) would depend on the probability distribution for r.

Acknowledgements. This work was supported by the Department of Energy (Office of Scientific Computing) under Contract No. DE-AS05-82ER12026.

REFERENCES

[1] J. P. Eckmann. *Rev. Mod. Phys.* **53** (1981), 643-654.
[2] M. J. Feigenbaum. *J. Stat. Phys.* **19** (1978), 25-62.
[3] C. Grebogi, E. Ott & J. A. Yorke. *Phys. Rev. Lett.* **48** (1952), 1507-1510.
[4] C. Grebogi, E. Ott & J. A. Yorke. *Phys. Rev. Lett.* **50** (1983), 935-938.
[5] C. Grebogi, E. Ott & J. A. Yorke. *Physica* **7D** (1983), 181-200.
[6] J. Guckenheimer & P. Holmes. *Nonlinear Oscillations, Dynamical Systems and Bifurcations of Vector Fields.* Springer-Verlag: New York, 1983.
[7] J. L. Kaplan & J. A. Yorke. In *Functional Differential Equations and Approximation of Fixed Points.* Lecture Notes in Mathematics, 730. Springer-Verlag: New York, 1979, p. 228.
[8] E. Ott. *Rev. Mod. Phys.* **53** (1981), 655-671; H. L. Swinney. *Physica* **7D**, (1983), 3-15 and references therein.
[9] Y. Pomeau & P. Manneville. *Comm. Math. Phys.* **74** (1980), 189-197.
[10] J. A. Yorke & E. D. Yorke. *J. Stat. Phys.* **21** (1979), 263-277.